processes

MDPI

Article

Enhancement of Tensile Strength of Coconut Shell Ash Reinforced Al-Si Alloys: A Novel Approach to Optimise Composition and Process Parameters Simultaneously

M. Poornesh [1], Shreeranga Bhat [1], Pavana Kumara Bellairu [1] and Olivia McDermott [2,*]

[1] St Josephs College of Engineering, Mangalore 575028, India; poorneshsjec@gmail.com (M.P.); shreeranga1981@gmail.com (S.B.); pavana1388@gmail.com (P.K.B.)
[2] College of Science & Engineering, University of Galway, H91 TK33 Galway, Ireland
* Correspondence: olivia.mcdermott@universityofgalway.ie

Abstract: The research presents a novel approach to develop high-strength functionally graded composite materials (FGCMs) by using recycled coconut shell ash (CSA) particles as reinforcement for a hypereutectic Al-Si alloy matrix. Using a centrifugal casting technique, test specimens are prepared for the study under ASTM standards. The optimal combination of materials to maximise the materials' overall tensile strength is obtained through the mixture methodology approach. The results show that CSA particles in the matrix material increase the tensile strength of the produced material. Process parameters, melting temperature and rotating speed were found to play a pivotal role in determining the tensile strength. A better tensile strength of the material is obtained when Al-Si = 90.5 wt%, CSA = 9.5 wt%, rotating speed = 800 RPM, and melting temperature = 800 °C; the proposed regression model developed has substantial predictability for tensile strength. This work presents a methodology for enhancing the tensile strength of FGCMs by optimising both the material composition and processing parameters. The achieved tensile strength of 197.4 MPa, at 800 RPM and 800 °C, for a concentration of 7.5 wt% CSA particles, makes these FGCMs suitable for use in multiple engineering sectors.

Keywords: functionally graded material; mixture methodology; cylinder liners; coconut shell ash; tensile strength

check for updates

Citation: Poornesh, M.; Bhat, S.; Bellairu, P.K.; McDermott, O. Enhancement of Tensile Strength of Coconut Shell Ash Reinforced Al-Si Alloys: A Novel Approach to Optimise Composition and Process Parameters Simultaneously. *Processes* **2024**, *12*, 1521. https://doi.org/10.3390/pr12071521

Academic Editor: Andrea Petrella

Received: 11 June 2024
Revised: 13 July 2024
Accepted: 15 July 2024
Published: 19 July 2024

Copyright: © 2024 by the authors. Licensee MDPI, Basel, Switzerland. This article is an open access article distributed under the terms and conditions of the Creative Commons Attribution (CC BY) license (https://creativecommons.org/licenses/by/4.0/).

1. Introduction

In all the commercially available internal combustion engines, cylinder heads play one of the most crucial roles since they provide a concealed chamber for combustion by mixing air and fuel, thus producing power for the vehicle. Therefore, to obtain peak efficiency, their design and material selection becomes crucial [1,2]. Due to their inherent characteristics, cast iron and steel have been widely employed in fabricating cylinder liners in most engines [3,4]. Due to its enhanced wear resistance properties, damping ability, and thermal conductivity, cast iron is one of the best material choices for use under high-pressure conditions and temperatures in cylinder heads [5,6]. Similarly, steel can be preferred as an engine material due to its strength and high-temperature capabilities [7].

Even though cast iron and steel are the most commonly used materials to fabricate cylinder liners of automobile engines, they have major drawbacks, such as a high weight, as well as other aspects. Most engines are bulky and must be able to perform under high energy, and the cylinder liners fabricated using cast iron have lower fuel efficiency. The carbon emission rate is high as well. A similar trend in the results is also observed in the engines that consist of steel cylinder heads [8,9]. Besides the high weight, cast iron and steel are prone to corrosion and rust, thus decreasing the engine's performance and lifespan. To overcome these drawbacks, automobile manufacturers prefer to use an alternative material

for producing cylinder liners that can deliver increased fuel efficiency, performance and increased longevity, and aluminium alloys are the best option out of all of them [10,11].

Because of their outstanding strength-to-weight ratio, excellent thermal conductivity, and low coefficient of thermal expansion, Al-Si alloys have become increasingly popular in recent years for usage in cylinder heads. These characteristics enable enhanced engine performance, increased fuel economy, and decreased emissions [12]. In addition to being low in cost compared with cast iron and steel, Al-Si alloys have better machinability and, hence, can be easily cast into complex shapes, allowing for greater design flexibility [10]. Al-Si alloys' combination of strength, low density, and thermal conductivity make them ideal for automotive parts, particularly cylinder heads requiring heat resistance and castability. Their lightweight nature further extends their use to engine blocks, gearboxes, and other components, meeting the auto industry's need for balance between weight reduction, strength, corrosion resistance, and affordability [13–15].

Indeed, as a standalone material, Al-Si alloy has numerous benefits for cylinder heads. Nevertheless, reinforcing the alloys can further enhance their existing properties, thus creating a composite structure [16]. Al-Si alloys can be reinforced with ceramic particles like SiC, Al_2O_3, and B_4C, enhancing their strength, durability, wear resistance and damping factors while increasing their weight [17–19]. Al-Si alloys are ideal for engine components due to their excellent thermal conductivity, which aids in heat dissipation from high-heat parts like cylinder heads [20,21]. This property makes them lightweight and thermally efficient, as shown in research by Weng et al. [22], Qi et al. [23] and Jia-ying Zhang et al. [24].

Introducing the ceramic reinforcement particles into the Al-Si melt during the preparation of the composite has proven to be beneficial by enhancing the overall properties and increasing the overall weight of the material. Research by Dias et al. [25] demonstrates a positive correlation between silicon concentration and the material's strength, hardness, and ductility. This highlights the crucial role of alloy composition in optimising cylinder head quality. Thus, the conventional approach is being redefined by adapting the concepts of sustainable practices. Moreover, recent studies show that reinforcing Al-Si alloys with agricultural wastes elevates the properties mentioned above and decreases the composite structure's overall weight. This can lead to increased fuel economy and fewer automobile emissions, rendering it a more environmentally friendly choice [26,27].

Using agricultural and industrial wastes has significantly increased the development of sustainable material research, since it provides novel opportunities by minimising environmental impacts. Coconut shell ash (CSA) is an abundantly available by-product that can be used as reinforcing particles for an aluminium-based composite material to obtain enhanced properties. Due to its high silica content and inherent hardness, it is best suited to use as reinforcing particles. The tensile strength, hardness, and, thus, wear resistance can be increased due to its inclusion, as exhibited in the work carried out by R. Siva Sankara Raju et al. [28] and Lakshmikanthan Purushothaman et al. [29]. Since the CSA particles are naturally lower in weight, they contribute mainly towards producing low-density composites, which can be used in applications where a high strength–low weight ratio is crucial.

Centrifugal casting is a viable option for fabricating cylinder heads utilising Al-Si alloys. The spinning mould in the operation creates a centrifugal force, accumulating the impurities in the mould's inner surface, thereby creating a cleaner and more homogenous structure [30]. Moreover, centrifugal casting allows for the production of cylinder heads with improved mechanical properties, as the directional solidification achieved through this process leads to a columnar grain structure, which is beneficial in terms of fatigue strength and resistance to thermal stresses [31]. Therefore, centrifugal casting can be a superior method for manufacturing high-quality and durable cylinder heads in the automotive industry. The centrifugal casting process involves various process parameters such as mould material, rotational speed, pouring temperature, cooling temperature, etc., which influence the final product quality by minimising defects and variations in the casting [32,33].

In order to improve the overall quality of the final products and or materials, it is essential to optimise the composition, since it directly influences the performance and reliability. Most of the material's properties, like strength, hardness, flexibility, ductility and resistance, are determined through the composition. Even minute changes in the composition can substantially vary the expected results, thus leading to subpar and even unwanted properties. In order to achieve consistent and high-performance results, it is important to carefully optimise the parameters of composite materials [34,35]. Balancing factors such as reinforcement amount, material composition, and processing is crucial [36]. Focusing solely on a single parameter overlooks the complexity involved and can result in suboptimal properties [37]. Instead, a multi-objective optimisation approach should be taken to achieve optimal strength, durability, and other desired properties. Techniques like the Grey Relation Analysis and Taguchi method can be employed for this purpose [35,38]. This holistic approach is beneficial across various industries, ranging from automotive to aerospace [34–38]. Mixture design methodology is often selected to address the complexities of determining the composition's best mixture. It is a statistical technique employed to obtain the optimum combination in a mixture so that the expected properties can be attained. As crucial as the optimisation of the composition is, it is equally important to optimise the parameters which affect the process conditions. Parameters are the set of conditions employed during the product's fabrication process, and thus, optimising them can result in better quality and performance. A noticeable gap in the research has been found, as the simultaneous optimisation of both composition and parameters has not been largely explored. The studies conducted by Arul Daniel et al. [35] and Juliana et al. [36] provide evidence of the effectiveness of the Taguchi–Grey Relation Analysis in optimising machining parameters for composite materials. Both studies achieved the objectives of minimising surface roughness and cutting force, while maximising material removal rate. Furthermore, Bao et al. [39] utilised mixture design to optimise wear resistance in PPESK composites, successfully reducing friction and wear through parameter variation. These studies collectively emphasise the efficiency of different optimisation techniques in enhancing the properties of composite materials.

Thus, based on the above discussion, the research aims to develop novel Al-Si alloys with superior tensile strength for industrial applications, using agricultural wastes. More specifically, it is intended to optimise the composition and process parameters simultaneously through the Mixture DOE approach. Moreover, the objective is to develop and validate an equation that helps academicians conduct further R&D activities.

2. Experimental Details

2.1. Selection of the Base Material

The base alloy for this study is a hypereutectic Al-18wt%Si alloy. The nominal chemical composition of the alloy is given in Table 1. Additionally, trace impurities that are commonly found in commercial alloys were present. The deliberate choice of a hypereutectic Al-Si alloy was based on its advantageous properties for cylinder liner applications. These properties include exceptional wear resistance, thermal conductivity, and a favourable strength-to-weight ratio. These particular properties are crucial for components that are exposed to the demanding operating conditions within an engine cylinder.

Table 1. Chemical composition of base alloy.

Element	Si	Cu	Mg	Fe	S	Others
Wt%	17.95	4.23	0.58	0.7	0.03	Remaining

2.2. Preparation of Coconut Shell Ash

Coconut shell ash is one of the most versatile materials available in nature. It finds a broad spectrum of applications, varying from gardening to pottery making and even construction [40,41]. The conventional method of producing ash begins with burning dried

coconut shells at a constant temperature. The process encourages reusing the coconut shells, which are generally considered waste, thus creating a more sustainable, eco-friendly substitute to conventional materials. The comprehensive technique for the production of coconut shell ash is given below:

Step 1: Collection of the Coconut Shells

The production process usually starts by collecting discarded coconut shells. These shells are the hard outer layers of the coconut, which are cast aside post the extraction of the inner pulp.

Step 2: Drying the Coconut Shells

The coconut shells were collected and initially scraped to remove any excess pulp from the inner core. Next, they were sun-dried for seven days, with ten hours of exposure each day, in order to make them easier to burn. To ensure uniform drying, the shells were flipped over daily. The process decreases the moisture content in the shells, making it easier to burn.

Step 3: Burning of the Shells

The burning of the dried coconut shells is usually carried out in a well-ventilated pit or perforated metal barrel. The shells are then completely burned to a temperature of 200–300 °C, thus obtaining charcoal [42]. In order to eliminate the high amount of carbon content in the charcoal, the second stage of burning is conducted under a controlled environment at a temperature of 700–800 °C, thus obtaining ash [43]. To achieve a more uniform particle size distribution, the ash particles are sieved, resulting in a final particle size range of approximately 70–80 microns.

2.3. Selection of Material Composition and Fabrication

The extensive literature survey, conducted to study the feasibility of agricultural waste as the reinforcing particles with metal matrix composites, revealed that the optimal test results were obtained when the amount of the reinforcement was generally in the range of 0–10 wt% [43–46]. This implies that the range of matrix material could feasibly vary across the entire spectrum of 0–100 wt%. Apart from the range of the reinforcing particles, fabrication parameters like melting temperature and rotation speed also influence the composite material's properties. The previous work revealed that an optimal melting temperature varying over 700–900 °C with a speed of 600–1000 rpm would yield better results [47,48]. Minitab software (https://www.minitab.com) is used to select the most effective material composition and perform the predetermined tests within the chosen ranges due to its ability to handle complex data. The extreme centroid mixture design technique in Minitab software uses various material composites, as shown in Table 2.

The composite material is then prepared in accordance with the material composition as well as the process parameter, as mentioned in Table 2. The composite material is prepared in two steps: melting the matrix material to the desired temperature using the stir casting technique and pouring the melt into the hollow cylindrical rotating shaft of a horizontal stir casting technique.

The commercially obtained raw Al-Si billets were then roughly cut and placed into a large graphite crucible, which was then placed inside an electrical furnace. Based on the melting temperature in Table 2, the billets were heated up to 700 °C and 800 °C [49,50]. At this juncture, hexachloroethane particles were carefully added to the molten mix. As a potent degassing agent, it purges the molten mix out of entrapped gases, thus paving a path for a more reliable casting process [51,52]. To improve the fluidity of the melt, the composite blend was enriched with 2 wt% of coarse magnesium particles [53]. The prepared and sieved reinforcing particles (CSA) were then preheated in a separate furnace to remove moisture from their surface. The stirrer was then slowly lowered inside the crucible containing the melt and rotated at a steady speed of 200 rpm [54,55]. The rotation created a vortex at the centre, and the reinforcing particles were poured into it. The mixing process was continued for a minimum of 10 minutes to ensure a maximum homogenous

mixing of reinforcing particles within the matrix material. In order to avoid chilling of the composite material, a hollow cylindrical mould with an inner diameter of 80 mm and a length of 120 mm was preheated. This preheating was carried out using a mechanical flame thrower, with the temperature set between 80 °C and 120 °C [56]. The mould was then rotated at the predetermined 600 or 800 RPM speeds. The stirred molten mix was slowly poured into this rotating mould to obtain the castings.

Table 2. Experimental layout obtained through Minitab software.

Experiment Layout									
Sample Number	**Al-18wt%Si (wt%)**	**Coconut Shell Ash (wt%)**	**Speed (RPM)**	**Temperature (°C)**	**Sample Number**	**Al-18wt%Si (wt%)**	**Coconut Shell Ash (wt%)**	**Speed (RPM)**	**Temperature (°C)**
A1	10	0	600	700	C1	10	0	600	800
A2	90	10	600	700	C2	90	10	600	800
A3	95	5	600	700	C3	95	5	600	800
A4	97.5	2.5	600	700	C4	97.5	2.5	600	800
A5	92.5	7.5	600	700	C5	92.5	7.5	600	800
B1	10	0	800	700	S1	10	0	800	800
B2	90	10	800	700	S2	90	10	800	800
B3	95	5	800	700	S3	95	5	800	800
B4	97.5	2.5	800	700	S4	97.5	2.5	800	800
B5	92.5	7.5	800	700	S5	92.5	7.5	800	800

2.4. Tensile Test

A computerised UTM is used to apply static load to assess the material's tensile strength. The tensile tests are carried out according to the ASTM E-8 standards [57,58]. The results are taken to ensure accuracy by averaging from 5 individual test readings.

3. Results and Discussion

3.1. XRD Analysis

In order to identify the crystalline contents present in the produced coconut shell ash particles, the particles are subjected to XRD analysis. The particles are exposed to an X-ray generator capable of 30 kv and a 4°/min scan speed. The particles present in the ash were then investigated using the X-ray diffraction method. The investigation revealed that the ash contains crystalline particles like SiO_2, Al_2O_3, and Fe_2O_3. As seen in Figure 1, a significant part of the ash comprised SiO_2 particles, with the highest peak closing at around 27. A comparison between the obtained XRD pattern and reference databases, as well as relevant studies on the composition of CSA [59,60], indicated the presence of crystalline phases such as SiO_2, Al_2O_3, and Fe_2O_3. This finding is consistent with the well-established knowledge of CSA composition, where these mineral phases are commonly identified due to the inherent presence of silicon, aluminum, and iron in the coconut shell precursor.

The crystalline phases found in the CSA greatly affect the properties of the composite materials produced. SiO_2, which was identified as the main component due to the distinct peaks observed around 27°, is renowned for its strength and stiffness. Adding these SiO_2

particles to the composite matrix improves its mechanical performance by reinforcing the structure and increasing resistance to deformation when under load.

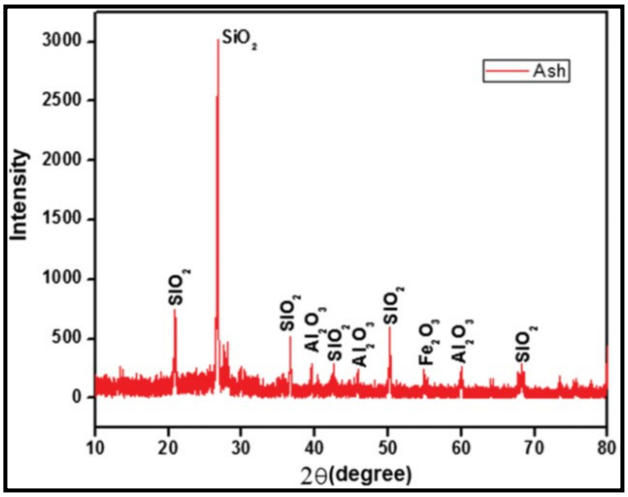


Figure 1. XRD Analysis of CSA particles.

The other contributing entities like Al_2O_3 and Fe_2O_3 also help make the matrix sturdier and more durable, thus indirectly helping improve the physical and mechanical properties of the produced composite materials. Although present in smaller quantities, Al_2O_3 and Fe_2O_3 can still contribute to the desirable properties of the composite. Alumina (Al_2O_3) is a highly wear-resistant ceramic material, and its presence in the CSA can enhance the composite's wear resistance. Similarly, ferric oxide (Fe_2O_3) can affect properties such as hardness and thermal stability, depending on its crystal structure and interaction with the matrix material. The chemical composition of the coconut shell ash particles obtained is mentioned in Table 3.

Table 3. Chemical composition of CSA particles.

Elements	Mass%
SiO_2	66.382
Al_2O_3	4.974
Fe_2O_3	15.741
CaO	3.428
K_2O	8.536
TiO	0.939

3.2. Tensile Strength

The tensile test was performed on all the composite specimens produced according to their specific conditions, as depicted in Table 2. The fabricated composite specimen at 600 RPM and 800 °C, with 100 wt% matrix and 0 wt% CSA particles, is shown in Figure 2. The tests were performed on the Tensometer according to the E-8 ASTM standard. Figure 3 shows the variation in the tensile strength due to the addition of the reinforcing particles for the composite specimens prepared at different speeds and temperatures.

It can be observed from Figure 3 that the addition of the reinforcing particles has a positive influence on the ultimate tensile strength of the produced composite specimen. The unreinforced composite material with 0 wt% of reinforcing particles was found to have the lowest strength, with an average value ranging from 112.3 MPa, whereas the composite with the reinforcing particles attained a strength of up to 197.4 MPa, with a total increase of 58.5% in strength. It is possible to comprehend the improvement in the tensile

strength when the Al-Si alloy is reinforced with CSA particles by considering the distinctive characteristics of the reinforcing particles and their interactions with the matrix material.



Figure 2. (**a**) Length-wise view of cylinder; (**b**) diametrical view of cylinder.

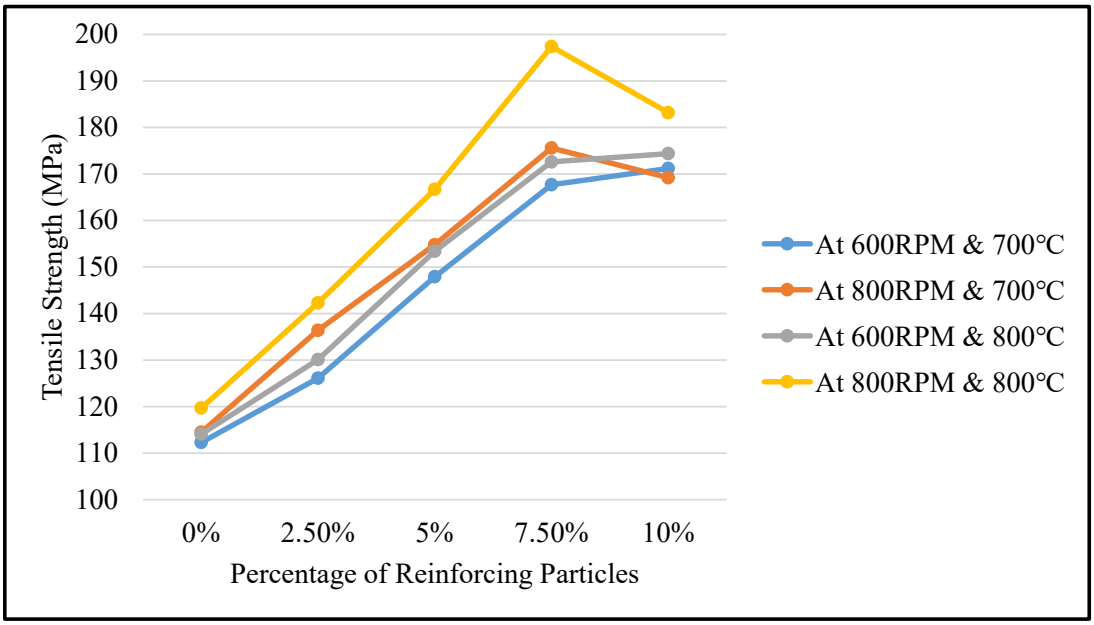


Figure 3. Variation in the ultimate tensile strength for composite specimen.

To begin with, it is evident that the innate hardness and rigidity of the reinforcing particles make them well-suited to reinforcement when dispersed within the Al-Si matrix. Due to these inherent properties, the reinforcing particles eventually support a portion of the load when the composite material is subjected to tensile forces [59]. Thus, allowing the force to be dispersed across a larger area reduces the probability of failure due to localised stresses. On the other hand, CSA particles help in strengthening the microstructural ability of the composite specimen. The dislocations and other flaws in the material tend to move when the material is deformed under load. The movement of the dislocations is comparatively easier in a single phase than in a multi-phase material, such as a composite [60]. In the composite material, CSA particles contribute to a secondary phase, which serves as the barrier to the motion of the dislocation. Due to this phenomenon, the particles prevent slip, which is one of the major reasons for deformations within the metals, as they restrict the path of dislocations. As a result of the restriction in motion, the prepared composite material becomes sturdier and stronger, thus increasing the tensile strength.

A slight increase in the results was observed when the rotation speed was increased by maintaining the same melting temperature. The centrifugal force acting on the rein-

forcing particles increases as the speed at which the mould rotates increases. A better distribution and alignment of the reinforcing particles is obtained within the matrix due to the centrifugal force pushing the particles towards the outer surface of the mould [61]. Due to this, the reinforcing particles can distribute the load better when the composite material is subjected to tensile loading. This improvement in the distribution can thereby influence the material's mechanical properties, such as tensile strength [62]. An increase in the rotating speed of the mould also leads to an increase in the cooling rate, which encourages the grain refinement in the matrix material during solidification. According to the Hall–Petch relationship, the smaller grains increase the amount of grain boundaries. These grain boundaries act as barriers to the dislocation movement when the material is subjected to tensile stresses [63,64]. A decrease in the porosity is noticed due to the increase in the centrifugal force in the composite material. Any voids in the material are squeezed out to the increased pressure, creating a denser and stronger composite with improved tensile strength.

It can be seen from Figure 3 that when the composite material is reinforced with 10 wt% of CSA particles, a small decrease is observed in the tensile strength. A marginal decrease of 3.6% has been noticed due to the addition of the reinforcing particles from 7.5 wt% to 10 wt%. This decrease can be attributed to various reasons, one of them being particle agglomeration. With the increase in the reinforcing particles, the tendency to cluster or agglomerate also increases, which leads to the irregular distribution of the reinforcement within the matrix. As the particle clusters increase within the matrix, the tensile stress of the composite decreases, as these clusters act as the stress concentrators to initiate the cracks [65,66].

At 600 RPM and 800 °C, it is evident that the inclusion of the CSA as reinforcing particles significantly increased the tensile strength of the composite. The reinforcing particles within the matrix disperse more evenly when the melting temperature of the matrix material is increased. At higher temperatures, the fluidity of the molten matrix material increases. This allows the reinforcing particles to move freely with the melt, thereby distributing itself more consistently [67,68]. When loaded under tensile stresses, the composite material, due to the homogenous dispersion of the reinforcing particles, will have an improved load-bearing capacity, boosting the tensile strength. The matrix and reinforcing phase bonding increases at higher temperatures [69]. The tensile strength of the produced composite material is increased through this improved bonding, which guarantees efficient load transfer from the matrix to the reinforcement, as observed in the results in Figure 2.

Elevating the processing temperatures is a compelling strategy to increase the tensile strength of the composite material. This improvement is mainly due to the matrix metal becoming more fluid. In this state, the metal is better able to wet and distribute the reinforcing particles, resulting in a more uniform and robust composite structure, ultimately leading to higher tensile strength. Additionally, incorporating hexachloroethane during the composite preparation is beneficial. It acts as a degassing agent, helping to remove flux and trapped gases. This not only improves the flow of the molten metal, but also reduces the formation of harmful voids and microcracks within the composite. Since these voids and cracks can act as stress concentrators during tensile loading, reducing them through effective degassing with hexachloroethane can greatly enhance the overall tensile strength [70].

At a higher speed and temperature of 800 RPM and 800 °C, it was observed that increasing the rotating speed of the centrifugal casting process exerts a higher centrifugal force on the molten mix. These higher forces, in return, help in the better distribution and eventual alignment of the reinforcing particles within the matrix, which optimises the load-sharing capability of the material under tensile loading [60]. A positive impact is observed in the tensile strength due to the increasing melting temperature. Improving the fluidity of the matrix material at higher temperatures facilitates better dispersion of the

reinforcing particles. This almost homogenous dispersion helps distribute the load more effectively, thus increasing the tensile strength [68].

It has been observed from Figure 4, that the composite material produced at 600 RPM and 700 °C exhibits an increase in yield strength. This increase in strength is mainly attributed to the inherent superior hardness and stiffness of CSA particles compared to the aluminium matrix, resulting in a dispersion of strengthening sites throughout the composite microstructure. These dispersed ceramic particles act as obstacles that dislocations, which are crucial for plastic deformation, must overcome during tensile loading. By overcoming this "pinning effect" caused by the CSA particles, a higher applied stress is required, ultimately leading to an enhanced yield strength. Furthermore, the presence of SiO_2 particles in CSA interacts with the aluminium matrix, facilitating the formation of strong interfacial phases at the CSA particle–matrix interface. These newly formed phases act as additional barriers to dislocation movement, further contributing to the strengthening effect [60,62].

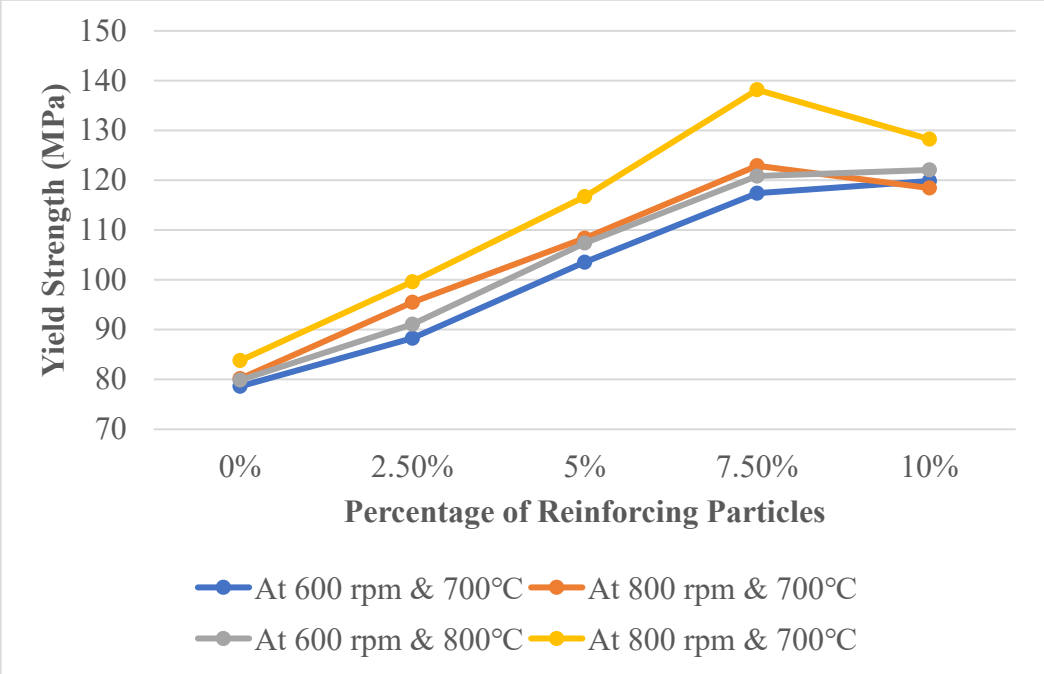


Figure 4. Variation in yield strength for composite specimen.

When the composite is prepared by increasing the rotating speed of the mould to 800 rpm while maintaining the same melting temperature, an increase in yield strength is observed. This is attributed to two crucial factors: enhanced particle distribution and a refined microstructure. Higher stirring speeds facilitate a more uniform dispersion of CSA particles throughout the matrix, thereby maximising the advantages of their strengthening mechanisms [66]. Moreover, the intense shear forces can result in a finer grain structure within the composite. These finer grains, combined with stronger particle–matrix bonding, additionally impede dislocation movement and bolster the overall yield strength.

By increasing the melting temperature from 700 °C to 800 °C, while keeping the rotating speed of the mould at 600 rpm, an increase in the yield strength of the composite material is observed. This can be attributed to two main factors. Firstly, the increased temperature enhances diffusion, resulting in stronger bonding between the CSA particles and the matrix. This stronger interface allows for better stress transfer and ultimately leads to a higher yield strength. Additionally, at a temperature of 700 °C, the matrix material is slightly softer, which provides less resistance to dislocations and may cause earlier yielding [68].

Finally, when the composite is produced at 800 rpm and 800 °C, the yield strength is found to be the highest in comparison to the other cases. It has been observed that, up to 7.5 wt% CSA, a higher stirring speed promotes better particle distribution and stronger bonding between the CSA particles and the matrix. This results in more efficient stress transfer and an increase in yield strength. However, exceeding 7.5 wt% CSA has detrimental effects. The CSA particles start to clump together, creating weak spots in the composite that initiate cracks at lower stress levels. Additionally, excessive CSA can hinder proper bonding with the aluminium matrix, further reducing the overall yield strength.

3.3. Mixture DOE

Figure 3 displays the results of the experiments conducted on tensile strength. According to the results shown in Figure 3, the tensile strength of Sample S4 is the highest, while that of Sample A1 is the lowest. Despite these findings, a conclusive choice regarding the optimal levels should not be made based only on the data provided, since complex interactions may exist between components. Therefore, a mixture design study (estimated regression coefficients for tensile) was conducted using Minitab's statistical analysis tools. The regression model was constructed using Minitab statistical software to analyse the relationship between the tensile strength of the composite material and the process parameters. The steps involved in constructing the regression model are as follows:

- Selection of Variables: The dependent variable selected for the regression analysis was tensile strength. The independent variables included the weight percentage of coconut shell ash (CSA), stirring speed, and melting temperature.
- Model Specification: A single regression analysis was performed to determine the relationship between the dependent and independent variables. The general form of the regression equation is:

$$Y = \beta_0 + \beta_1 X_1 + \in$$

  where Y represents the tensile strength, $X1$ represents the independent variable (e.g., weight percentage of CSA), $\beta 0$ is the intercept, $\beta 1$ is the coefficient of the independent variable, and ϵ is the error term.
- Significance Testing: The significance of the term in the regression model was evaluated using p-values. The term with a p-value less than 0.05 was considered statistically significant and included in the final model.
- Evaluation of Interactions: Although the primary focus was on single regression analysis, interaction effects between the independent variables were also assessed to determine their combined influence on tensile strength. Interaction terms were evaluated for their significance, and included in the model if they improved the model's predictive capability.
- Model Validation: The model was validated by examining the R-squared (R^2), adjusted R-squared (R^2 adj), and predicted R-squared (R^2 pred) values. These statistics indicate the proportion of variance explained by the model, adjusted for the number of predictors, and the model's predictive accuracy, respectively. High values of these statistics confirmed the model's robustness.
- Diagnostic Plots: Diagnostic plots, including residual plots and normal probability plots, were used to check the assumptions of the regression analysis, such as the linearity, independence, homoscedasticity, and normality of residuals. These plots confirmed that the assumptions were met, validating the reliability of the regression model.

Tables 4 and 5 show the results of the analysis. From this output, it can be concluded that interactions "Al-18wt%Si × Coconut Shell Ash", "Coconut Shell Ash × Speed", and "Al-18wt%Si × Coconut Shell Ash × Speed" are significant at a 5% level of significance (since p-value < 0.05). In addition, a synergistic effect is indicated by a positive coefficient of third-order interaction (Table 4).

Table 4. Estimated regression coefficients for tensile strength (MPa) (component proportions).

Term	Coef	SE-Coef	T-Value	*p*-Value	VIF
Al-18wt%Si	112.70	1.20	-	-	4.00
Coconut Shell Ash	−3770	491	-	-	2787.57
Al-18wt%Si × Coconut Shell Ash	5036	545	9.25	**0.000** *	2882.43
Al-18wt%Si × Speed	1.61	1.20	1.35	0.182	4.00
Coconut Shell Ash × Speed	−1815	491	−3.70	**0.000** *	2787.57
Al-18wt%Si × Coconut Shell Ash × Speed	2024	545	3.72	**0.000** *	2882.43
Al-18wt%Si × Temperature	1.33	1.20	1.11	0.270	4.00
Coconut Shell Ash × Temperature	−534	491	−1.09	0.279	2787.57
Al-18wt%Si × Coconut Shell Ash × Temperature	637	545	1.17	0.245	2882.43

* Significant at a 5% confidence interval.

Table 5. Analysis of variance for tensile strength (MPa) (component proportions).

Source	DF	Seq-SS	Adj-SS	Adj-MS	F-Value	*p*-Value
Regression	8	59,731.3	59,731.3	7466.41	230.12	**0.000** *
Component Only						
Linear	1	52,733.2	2033.3	2033.32	62.67	**0.000** *
Quadratic	1	2773.5	2773.5	2773.51	85.48	**0.000** *
Al-18wt%Si × Coconut Shell Ash	1	2773.5	2773.5	2773.51	85.48	**0.000** *
Component × Speed						
Linear	2	1925.2	968.8	484.42	14.93	**0.000** *
Al-18wt%Si × Speed	1	1914.1	58.7	58.71	1.81	0.182
Coconut Shell Ash × Speed	1	11.1	443.3	443.33	13.66	**0.000** *
Quadratic	1	448.2	448.2	448.16	13.81	**0.000** *
Al-18wt%Si × Coconut Shell Ash × Speed	1	448.2	448.2	448.16	13.81	**0.000** *
Component × Temperature						
Linear	2	1806.7	173.1	86.55	2.67	**0.075** **
Al-18wt%Si × Temperature	1	1583.0	40.0	39.96	1.23	0.270
Coconut Shell Ash × Temperature	1	223.7	38.4	38.41	1.18	0.279
Quadratic	1	44.4	44.4	44.45	1.37	0.245
Al-18wt%Si × Coconut Shell Ash × Temperature	1	44.4	44.4	44.45	1.37	0.245
Residual Error	91	2952.6	2952.6	32.45		
Total	99	62,683.9				

* Significant at 5% confidence interval; ** Significant at 10% confidence interval.

A residual analysis (Figure 5) is carried out to verify further that the model adequately describes outcomes. Figure 5 shows that the residuals are randomly distributed and have constant variance, the first requirement for model validation. The residual vs. order plot confirms that the residuals do not follow any discernible patterns, suggesting no relationships. This clarifies the second assumption that the residuals are independent. Last, the normal probability plot verifies the third premise, which states that the residuals have a normal distribution.

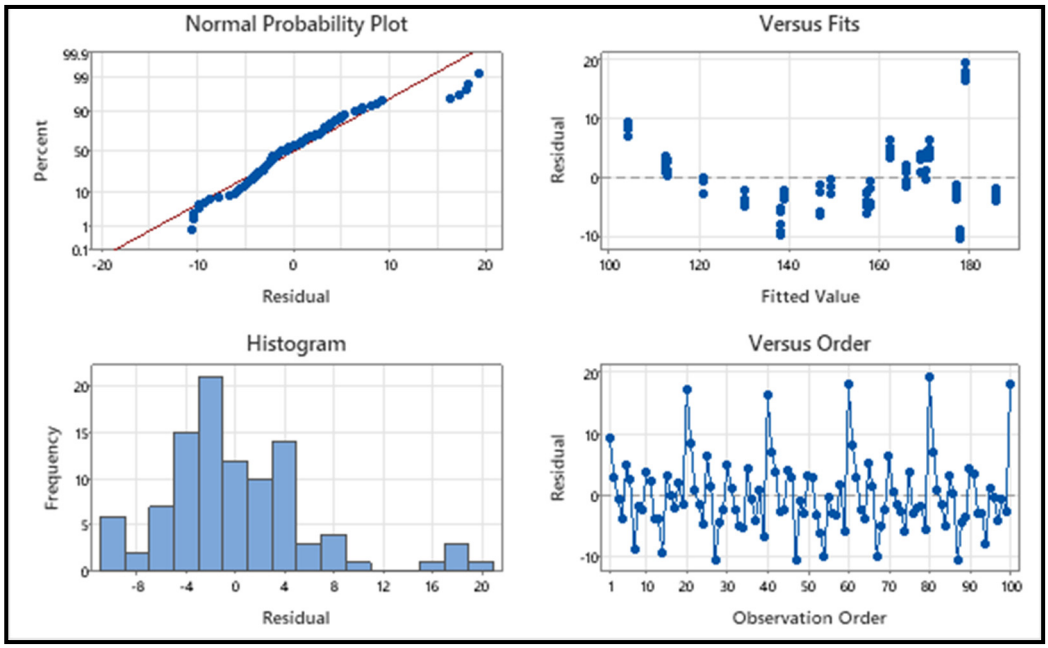


Figure 5. Residual analysis for tensile strength (MPa).

In addition, the ANOVA (Table 5) cites that the quadratic model (Al-18wt%Si × Coconut Shell Ash × Speed) is statistically significant (p-value < 0.05). Moreover, the pareto chart of the standardised effects (Figure 6) indicates that "Al-18wt%Si (A)", "Speed (C)", "Temperature (D)", and "Al-18wt%Si × Coconut Shell Ash (A × B)" significantly affect the tensile strength.

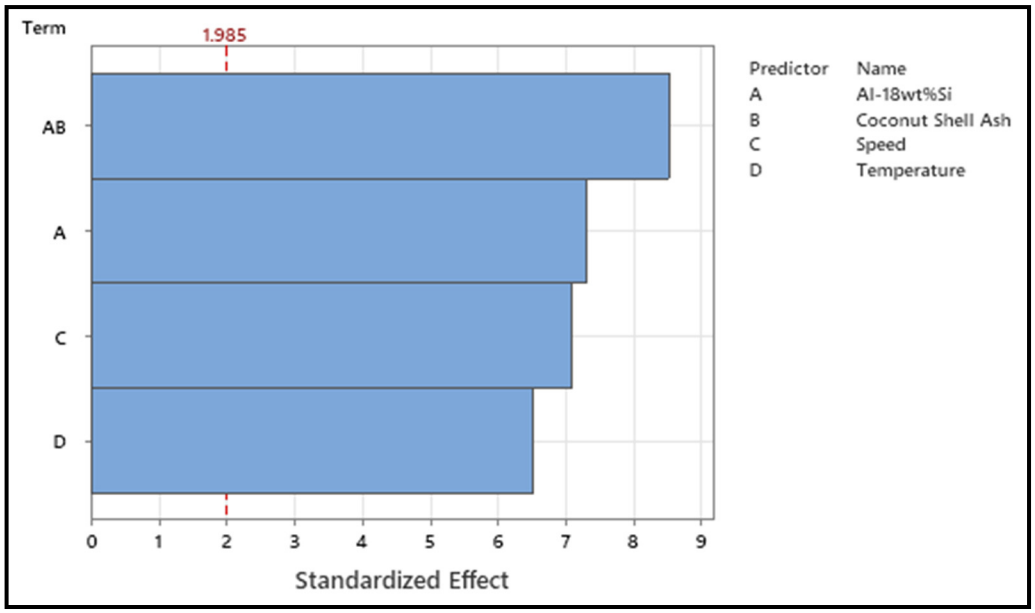


Figure 6. Pareto chart of the standardised effect.

Based on the findings above, a quadratic model was constructed using regression analysis to identify the model's coefficients by deleting the insignificant factors at the 5% level. Table 6 presents the predictive model for further research work. With a confidence level of 95%, this equation facilitates the prediction of the flexural strength of innovative materials for academics and practitioners. By using this prediction model, it is possible to modify the material's tensile strength in accordance with the specific demands of the

application. Furthermore, as shown by the R-square (adj) value in Table 5, the model adequately accounts for 93.97% of the variance in tensile strength; consequently, the model provides an excellent fit to the data. An R-square (pre) score of 93.63 percent further indicates that the model has considerable predictability.

Table 6. Regression equation.

Tensile Strength (MPa) = −3861 + 38.83 (Al-18wt%Si) + 0.04384 (Speed) + 0.0806 (Temperature) + 0.5036 (Al-18wt%Si) × (Coconut Shell Ash)			
Model Summary			
S	**R-sq**	**R-sq (adj)**	**R-sq (pred)**
6.18099	94.21%	93.97%	93.63%

3.4. Determination of Optimal Composition

The experimental tensile strength results obtained are further used to determine the optimum composition of the bend, and a response optimiser is used for the analysis. While doing so, the tensile strength values are taken as responses, and the design layout is taken as the predictor. Since the goal is to determine the optimal composition to maximise the tensile strength, the target value and upper boundary for the optimisation are taken as the maximum observed value (198.7 MPa). The lower boundary is taken as the minimum value (111.4 MPa) from the experimental result (Table 7). The response optimisation plot was thus obtained, indicating that the best possible composition for tensile strength within specified optimisation parameters is Al-18wt%Si = 90.5 wt%, coconut shell ash = 9.5 wt%, speed = 800 RPM, and temperature = 800 °C.

Table 7. Parameters for the optimisation.

Tensile Strength (MPa) = −3861 + 38.83 (Al-18wt%Si) + 0.04384 (Speed) + 0.0806 (Temperature) + 0.5036 (Al-18wt%Si) × (Coconut Shell Ash)			
Model Summary			
S	**R-sq**	**R-sq (adj)**	**R-sq (pred)**
6.18099	94.21%	93.97%	93.63%

For Figures 6 and 7, a comparison with similar published articles offers valuable insights into the optimisation and enhancement of composite materials. Our study focuses on the enhancement of tensile strength in coconut shell ash (CSA) reinforced Al-Si alloys by optimising both composition and process parameters. Figure 4 in our study highlights the improvements in tensile strength, while Figure 5 shows the microstructural changes due to CSA reinforcement.

The study by Poornesh et al. [18] employs a multi-objective approach to optimise Al-Si composites reinforced with SiC particles. Their outcome demonstrates a notable increase in hardness and tensile strength with increasing SiC content, similar to the enhancements observed in our study with the CSA reinforcement in the pareto chart of the standardised effects. The response optimiser plot in this study shows the microstructural changes with a more uniform distribution and better bonding of SiC particles under optimised conditions, highlighting the critical role of reinforcement type and process optimisation in improving composite properties. Further, Bellairu et al. [71] examines the use of natural fibers as reinforcement in composites, showing that optimised natural fiber content significantly improves mechanical properties. The tensile strength improvements and microstructural uniformity observed in our study with CSA reinforcement align with the findings of this study, which also emphasises the importance of optimising natural reinforcement content and process parameters for substantial mechanical property enhancements by using the response optimiser plot and pareto chart. Besides, Proornesh et al. [17]

explores the optimisation of mechanical properties in composite materials using various reinforcement materials and techniques. Similar to our findings, the study shows that optimising reinforcement content and process parameters leads to significant improvements in tensile strength and a more uniform microstructure. The comparative analysis reveals that different reinforcement materials, such as natural fibers and SiC, can achieve similar enhancements in mechanical properties when optimal conditions are met. Eventually, the comparison with these studies underscores that while different reinforcement materials like CSA, SiC, and natural fibers are used, the optimisation of composition and process parameters consistently results in enhanced mechanical properties and improved microstructural characteristics. This reinforces the versatility and importance of optimising composite materials for achieving superior performance.

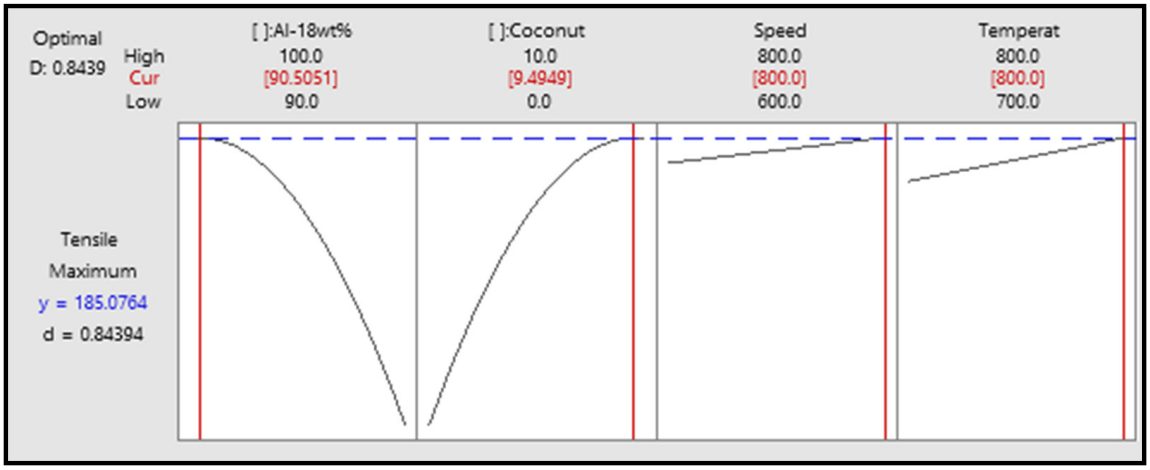


Figure 7. Response optimiser plot.

The composite material with the optimal composition showed a recorded percentage elongation of 4.16%, indicating limited ductility. There are several factors that can be attributed to this relatively low value. The addition of CSA particles to the aluminum matrix greatly improves the strength properties of the material, such as tensile and yield strength. However, this reinforcement often leads to a decrease in ductility. This is because the hard and brittle CSA particles create stress points, which hinder the material's ability to deform and increase the likelihood of cracks forming. The reduced ductility of the hypereutectic Al-Si alloy matrix is due to its composition. Additionally, the presence of brittle primary silicon particles further restricts the material's ability to undergo plastic deformation without fracturing. Furthermore, the composition of the hypereutectic Al-Si matrix, which includes brittle primary silicon phases, worsens this behavior. As a result, the composite cylinder liner provides excellent wear resistance and load-bearing capacity but sacrifices ductility. This makes it ideal for applications that prioritise these properties.

After completing the optimisation process, a composite cylinder using the optimal mixture composition is fabricated. Subsequently, a microstructure analysis is conducted on the cylinder to assess the distribution of particles. Micrographs were taken at 2 mm intervals from the outer diameter, as depicted in Figure 8a–f. These images highlight the influence of centrifugal forces and varying particle densities. It is evident from the images that the denser CSA particles were pushed towards the outer regions due to the centrifugal forces experienced during the casting process. As a result, the particle distribution throughout the cylinder is uneven, with higher concentrations of CSA compared to aluminum and silicon.

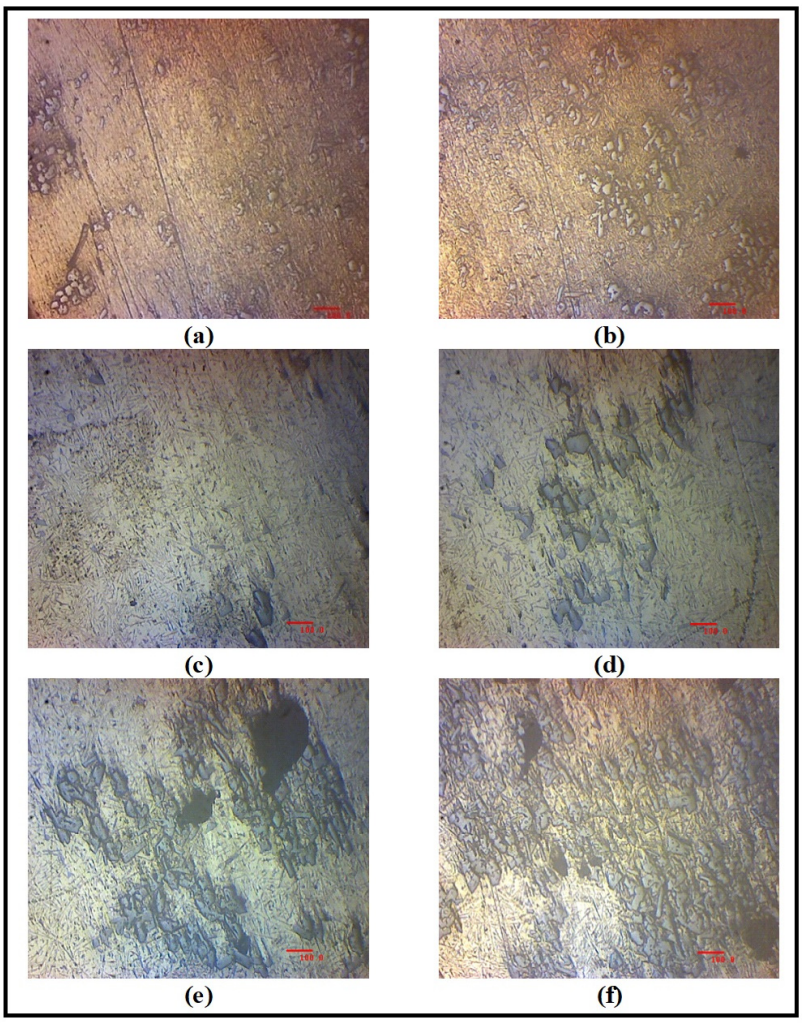


Figure 8. (**a**–**f**): Optical microstructural images of the composite prepared using optimal mixture combination.

The chemical composition of the composite material produced under optimised process parameters is presented in Table 8.

Table 8. Chemical composition of the composite material.

Elements	Wt%	Elements	Wt%
Si	16.15	Al_2O_3	0.47
Cu	3.80	Fe_2O_3	1.49
Mg	0.522	CaO	0.32
Fe	0.63	K_2O	0.81
S	0.02	TiO	0.089
SiO_2	6.30	Others	Remaining

Figure 8a confirms the expected distribution of particles resulting from centrifugal casting. The denser CSA particles, along with the primary silicon from the Al-18wt%Si matrix, are concentrated towards the outer diameter. This aligns with the concept of directional solidification, which is caused by the chilling effect of the mold. The molten metal rapidly solidifies upon contact with the mold, effectively trapping denser phases like CSA and primary silicon towards the outer edges. In contrast, the eutectic silicon, with

its needle-like structure, is dispersed throughout the matrix in a more uniform manner. This observed microstructure, achieved using the optimal mixture composition, suggests improved properties for the composite cylinder.

4. Conclusions

The current research has proposed and validated a roadmap to combine the concepts of mechanical engineering, material science and statistical techniques to ensure robust composition design and optimisation. The step-by-step approach demonstrated in the study helps practitioners and academicians create novel composite materials and validate the mechanical properties from a multidisciplinary perspective. The mixture methodology design of experiments employed is an excellent tool for addressing multiple process parameters and generating robust predictive models. The following inferences can be drawn after the careful study and analysis of the current research:

i. Usually, discarded coconut shells can be effectively used to produce novel composite materials, thus building a new sustainable future and helping contribute to the circular economy.
ii. The XRD Analysis of the coconut shell ash particles reveals the presence of crystalline particles, such as SiO_2, Al_2O_3 and Fe_2O_3, among others.
iii. The composite materials can be effectively produced by combining stir and centrifugal casting.
iv. The results of the tensile tests performed on the produced composite materials revealed that adding reinforcing particles increased the tensile strength. The inclusion of the reinforcing particles acts as motion barriers to the dislocation when subjected to loading, thus slowing the fracture process and increasing the strength. The tensile strength has decreased slightly when reinforced with 10wt% of reinforcing particles, which is attributed to improper mixing and settlement of the particles.
v. The predictive model developed through the statistical analysis shows high predictability levels (R2 = 93.63%).
vi. The study concludes that the composite materials produced at Al-18wt%Si = 90.5 wt%, coconut shell ash = 9.5 wt%, speed = 800 RPM, and temperature = 800 °C will give superior results.

Within the Design for Manufacturing (DFM) realm and from the perspective of probable industrial applications, the study explores a multidisciplinary approach to optimising composite materials' composition and process parameters. While the current research focuses on optimising the material's tensile properties, the researchers advocate extending it to other facets, such as hardness, density, toughness, tribological and thermal properties. The study aims to comprehensively understand how the materials behave under various properties, thus increasing the knowledge base. This knowledge base can then be used to unlock the composite material's potential for society's benefit by offering its valuable insights to academia and industries.

Author Contributions: Conceptualisation, M.P., S.B., P.K.B. and O.M.; methodology, M.P., S.B. and P.K.B.; software, M.P., S.B. and P.K.B.; validation, M.P., S.B., P.K.B. and O.M.; formal analysis, S.B. and P.K.B.; investigation, M.P. and O.M.; data curation, M.P., S.B. and P.K.B.; writing—original draft preparation, M.P., S.B., P.K.B. and O.M.; writing—review and editing, P.K.B. and O.M.; supervision, O.M.; project administration, S.B. and P.K.B. All authors have read and agreed to the published version of the manuscript.

Funding: This research received no external funding.

Data Availability Statement: Data are available upon request from the authors.

Conflicts of Interest: The authors declare no conflicts of interest.

References

1. Reitz, R.D.; Ogawa, H.; Payri, R.; Fansler, T.; Kokjohn, S.; Moriyoshi, Y.; Agarwal, A.K.; Arcoumanis, D.; Assanis, D.; Bae, C.; et al. IJER editorial: The future of the internal combustion engine. *Int. J. Engine Res.* **2020**, *21*, 3–10. [CrossRef]
2. Yip, H.L.; Srna, A.; Yuen, A.C.Y.; Kook, S.; Taylor, R.A.; Yeoh, G.H.; Medwell, P.R.; Chan, Q.N. A Review of Hydrogen Direct Injection for Internal Combustion Engines: Towards Carbon-Free Combustion. *Appl. Sci.* **2019**, *9*, 4842. [CrossRef]
3. Guesser, W.; Cabezas, C.; Guedes, L.; Zanatta, A. High Temperature Strength of Cast Irons for Cylinder Heads. *Mater. Sci. Forum* **2018**, *925*, 385–392. [CrossRef]
4. Pan, S.; Zeng, F.; Su, N.; Xian, Z. The effect of niobium addition on the microstructure and properties of cast iron used in cylinder head. *J. Mater. Res. Technol.* **2020**, *9*, 1509–1518. [CrossRef]
5. Abdou, S.; Elkaseer, A.; Kouta, H.; Qudeiri, J.A. Wear behaviour of grey cast iron with the presence of copper addition. *Adv. Mech. Eng.* **2018**, *10*, 1–8. [CrossRef]
6. Holmgren, D. Review of thermal conductivity of cast iron. *Int. J. Cast Met. Res.* **2005**, *18*, 331–345. [CrossRef]
7. Pierce, D.; Haynes, A.; Hughes, J.; Graves, R.; Maziasz, P.; Muralidharan, G.; Shyam, A.; Wang, B.; England, R.l.; Daniel, C. High temperature materials for heavy duty diesel engines: Historical and future trends. *Prog. Mater. Sci.* **2019**, *103*, 109–179. [CrossRef]
8. Hirz, M.; Nguyen, T.T. Life-Cycle CO_2-Equivalent Emissions of Cars Driven by Conventional and Electric Propulsion Systems. *World Electr. Veh. J.* **2022**, *13*, 61. [CrossRef]
9. Salonitis, K.; Jolly, M.; Pagone, E.; Papanikolaou, M. Life-Cycle and Energy Assessment of Automotive Component Manufacturing: The Dilemma Between Aluminum and Cast Iron. *Energies* **2019**, *12*, 2557. [CrossRef]
10. Javidani, M.; Larouche, D. Application of Cast Al-Si Alloys in Internal Combustion Engine Components. *Int. Mater. Rev.* **2014**, *59*, 132–158. [CrossRef]
11. Zhang, W.; Xu, J. Advanced lightweight materials for Automobiles: A review. *Mater. Des.* **2022**, *221*, 110994. [CrossRef]
12. Bolibruchová, D.; Širanec, L.; Matejka, M. Selected Properties of a Zr-Containing $AlSi_5Cu_2Mg$ Alloy Intended for Cylinder Head Castings. *Materials* **2022**, *15*, 4798. [CrossRef]
13. Niu, G.; Wang, Y.; Zhu, L.; Ye, J.; Mao, J. Fluidity of casting Al–Si series alloys for automotive light-weighting: A systematic review. *Mater. Sci. Technol.* **2022**, *38*, 902–911. [CrossRef]
14. Khan, A.; Kaiser, M.; Kaiser, M.; Saraçyakupoğlu, T. Wear studies on Al-Si automotive alloy under dry, fresh and used engine oil sliding environments. *Res. Eng. Struct. Mater.* **2023**, *9*, 1–18. [CrossRef]
15. Smokvina Hanza, S.; Vrsalović, L.; Štic, L.; Liverić, L. Corrosion investigations of Al-Si casting alloys in 0.6 M NaCl solution. *Eng. Rev.* **2021**, *41*, 115–123. [CrossRef]
16. Poornesh, M.; Bhat, S.; Gijo, E.V.; Bellairu, P.K. Enhancing the tensile strength of SiC reinforced aluminium-based functionally graded structure through the mixture design approach. *Int. J. Struct. Integr.* **2022**, *13*, 150–163. [CrossRef]
17. Poornesh, M.; Bhat, S.; Gijo, E.V.; Bellairu, P.K.; McDermott, O. Multi-Response Modelling and Optimisation of Mechanical Properties of Al-Si Alloy Using Mixture Design of Experiment Approach. *Processes* **2022**, *10*, 2246. [CrossRef]
18. Poornesh, M.; Bhat, S.; Gijo, E.V.; Bellairu, P.K. Multi-objective modelling and optimization of Al–Si–SiC composite material: A multi-disciplinary approach. *Multiscale Multidiscip. Model. Exp. Des.* **2022**, *5*, 53–66. [CrossRef]
19. Polat, S.; Sun, Y.; Çevi, E.; Colijn, H. Microstructure and synergistic reinforcing activity of GNPs-B4C dual-micro and nano supplements in Al-Si matrix composites. *J. Alloys Compd.* **2019**, *806*, 1230–1241. [CrossRef]
20. Qian, G.; Sun, L.; Chen, H.; Wang, Z.; Wei, K.; Ma, W. Enhancing impurities removal from Si by controlling crystal growth in directional solidification refining with Al–Si alloy. *J. Alloys Compd.* **2020**, *820*, 153300. [CrossRef]
21. Qi, M.; Kang, Y.; Qiu, Q.; Tang, W.; Li, J.; Li, B. Microstructures, mechanical properties, and corrosion behavior of novel high-thermal-conductivity hypoeutectic Al-Si alloys prepared by rheological high pressure die-casting and high pressure die-casting. *J. Alloys Compd.* **2018**, *749*, 487–502. [CrossRef]
22. Li, Q.; Zhao, S.; Li, B.; Zhu, Y.; Liu, J.; Liu, D.; Lan, Y.; Xia, T. Modification of multi-component Al–Si casting piston alloys by addition of rare earth yttrium. *Mater. Res. Express* **2019**, *6*, 106525. [CrossRef]
23. Weng, W.; Nagaumi, H.; Sheng, X.; Fan, W.; Chen, X.; Wang, X. Influence of Silicon Phase Particles on the Thermal Conductivity of Al-Si Alloys. In *Light Metals 2019*; Chesonis, C., Ed.; Springer: Cham, Switzerland, 2019; pp. 193–198.
24. Zhang, J.Y.; Zuo, L.J.; Jian FE, N.G.; Bing, Y.E.; Kong, X.Y.; Jiang, H.Y.; Ding, W.J. Effect of thermal exposure on microstructure and mechanical properties of Al−Si−Cu−Ni−Mg alloy produced by different casting technologies. *Trans. Nonferrous Met. Soc. China* **2020**, *30*, 1717–1730. [CrossRef]
25. Dias, M.; Oliveira, R.; Kakitani, R.; Cheung, N.; Henein, H.; Spinelli, J.E.; Garcia, A. Effects of solidification thermal parameters and Bi doping on silicon size, morphology and mechanical properties of Al-15wt.% Si-3.2wt.% Bi and Al-18wt.% Si-3.2wt.% Bi alloys. *J. Mater. Res. Technol.* **2020**, *9*, 3460–3470. [CrossRef]
26. Dixit, P.; Suhane, A. Aluminum metal matrix composites reinforced with rice husk ash: A review. *Mater. Today Proc.* **2022**, *62*, 4194–4201. [CrossRef]
27. Harish, T.M.; Mathai, S.; Cherian, J.; Mathew, K.M.; Thomas, T.; Prasad, K.V.; Ravi, V.C. Development of aluminium 5056/SiC/bagasse ash hybrid composites using stir casting method. *Mater. Today Proc.* **2020**, *27*, 2635–2639. [CrossRef]
28. Raju, S.; Siva, B. Fabrication and tribological studies of Al-CSA composite using RSM. *Int. J. Mater. Eng. Innov.* **2021**, *12*, 83. [CrossRef]

29. Purushothaman, L.; Balakrishnan, P. Wear and corrosion behavior of coconut shell ash (CSA) reinforced Al6061 metal matrix composites. *Mater. Test.* **2020**, *62*, 77–84. [CrossRef]
30. Saleh, B.; Ji, B.; Fathi, R.; Guo, S.; Ahmed, M.H.; Jiang, J.; Ma, A. Utilization of machining chips waste for production of functionally gradient magnesium matrix composites. *J. Mater. Process. Technol.* **2022**, *308*, 117702. [CrossRef]
31. De la Rocha, M.R.; Virginie, M.; Khodakov, A.; Pollo, L.D.; Marcílio, N.R.; Tessaro, I.C. Preparation of alumina based tubular asymmetric membranes incorporated with coal fly ash by centrifugal casting. *Ceram. Int.* **2021**, *47*, 4187–4196. [CrossRef]
32. Mohapatra, S.; Sarangi, H.; Mohanty, U.K. Effect of processing factors on the characteristics of centrifugal casting. *Manuf. Rev.* **2020**, *7*, 26. [CrossRef]
33. Liu, W.Y.; Zhang, J.B.; Jin, Y.M.; Hu, T.T.; Chen, T.T.; Xiao, X.P.; Yan, L.M. Microstructure and properties of Ti_3SiC_2/Al–Si composites synthesized by spark plasma sintering. *Mater. Res. Express* **2017**, *4*, 116521. [CrossRef]
34. Prakash, J.U.; Rubi, C.S.; Rajkumar, C.; Juliyana, S.J. Multi-objective drilling parameter optimization of hybrid metal matrix composites using grey relational analysis. *Mater. Today Proc.* **2021**, *39*, 1345–1350. [CrossRef]
35. Daniel, S.A.A.; Pugazhenthi, R.; Kumar, R.; Vijayananth, S. Multi objective prediction and optimization of control parameters in the milling of aluminium hybrid metal matrix composites using ANN and Taguchi -grey relational analysis. *Def. Technol.* **2019**, *15*, 545–556. [CrossRef]
36. Juliyana, S.J.; Prakash, J.U.; Čep, R.; Karthik, K. Multi-Objective Optimization of Machining Parameters for Drilling LM_5/ZrO_2 Composites Using Grey Relational Analysis. *Materials* **2023**, *16*, 3615. [CrossRef] [PubMed]
37. Sapkota, G.; Ghadai, R.K.; Das, S.; Das, P.P.; Chakraborty, S. A comparative study on multi-objective optimization of drilling of hybrid aluminium metal matrix composite. *Int. J. Interact. Des. Manuf. (IJIDeM)* **2023**, *17*, 3177–3187. [CrossRef]
38. Kumar, A.; Grover, N.; Manna, A.; Kumar, R.; Chohan, J.S.; Singh, S.; Singh, S.; Pruncu, C.I. Multi-Objective Optimization of WEDM of Aluminum Hybrid Composites Using AHP and Genetic Algorithm. *Arab. J. Sci. Eng.* **2022**, *47*, 8031–8043. [CrossRef]
39. Bao, Q.; Li, N.; Feng, J.; Yan, S.; Ma, G.; Wang, B.; Cheng, S.; Hao, H.; Liu, C.; Zhang, S.; et al. Using mixture design approach for modeling and optimizing tribology properties of PPESK composites. *Compos. Part A Appl. Sci. Manuf.* **2022**, *163*, 107256. [CrossRef]
40. Luhar, S.; Cheng, T.-W.; Luhar, I. Incorporation of natural waste from agricultural and aquacultural farming as supplementary materials with green concrete: A review. *Compos. Part B Eng.* **2019**, *175*, 107076. [CrossRef]
41. He, J.; Kawasaki, S.; Achal, V. The Utilization of Agricultural Waste as Agro-Cement in Concrete: A Review. *Sustainability* **2020**, *12*, 6971. [CrossRef]
42. Awogbemi, O.; Von Kallon, D.V. Application of biochar derived from crops residues for biofuel production. *Fuel Commun.* **2023**, *15*, 100088. [CrossRef]
43. Harish, T.M.; Mathai, S.; George, M.; Harisankar, M.; Francis, B. Development of aluminium 5083/B4C/carbonized coconut shell ash hybrid composite using friction stir processing. *Mater. Today Proc.* **2023**, *72*, 3149–3153. [CrossRef]
44. Kumar, A.; Nirala, A.; Singh, V.P.; Sahoo, B.K.; Singh, R.C.; Chaudhary, R.; Dewangan, A.K.; Gaurav, G.K.; Klemes, J.J.; Liu, X. The utilisation of coconut shell ash in production of hybrid composite: Microstructural characterisation and performance analysis. *J. Clean. Prod.* **2023**, *398*, 136494. [CrossRef]
45. Panda, B.; Niranjan, C.A.; Vishwanatha, A.D.; Harisha, P.; Chandan, K.R.; Kumar, R. Development of Novel Stir Cast Aluminium Composite with modified Coconut Shell Ash Filler. *Mater. Today Proc.* **2020**, *22*, 2715–2724. [CrossRef]
46. Kolappan, S.; Arunkumar, T.; Mohanavel, V.; Subramani, K.; Kailasanathan, C.; Kumaran, P.; Subbiah, R.; Kumar, S.S. Experimental investigation on stir casted hybrid composite AA7068 with SiC and coconut shell fly ash. *Mater. Today Proc.* **2022**, *62*, 5540–5545. [CrossRef]
47. Jenish, I.; Veeramalai Chinnasamy, S.G.; Basavarajappa, S.; Indran, S.; Divya, D.; Liu, Y.; Sanjay, M.R.; Siengchin, S. Tribo-Mechanical characterization of carbonized coconut shell micro particle reinforced with Cissus quadrangularis stem fiber/epoxy novel composite for structural application. *J. Nat. Fibers* **2022**, *19*, 2963–2979. [CrossRef]
48. Kadaru, S.K.R.; Kannan, M.; Karthikeyan, R. Preparation and investigation of wear and corrosion behaviour of Al 7475/CSA/Graphite hybrid metal matrix composites. *Adv. Mater. Process. Technol.* **2023**, 1–13. [CrossRef]
49. Ranjan, S.; Jha, P.K. Investigation on the thermodynamic stability of phases evolved in Al-based hybrid metal matrix composite fabricated using in-situ stir casting route. *J. Manuf. Process.* **2023**, *95*, 14–26. [CrossRef]
50. Zhang, P.; Zhang, W.; Du, Y.; Wang, Y. High-performance Al-1.5 wt% Si-Al_2O_3 composite by vortex-free high-speed stir casting. *J. Manuf. Process.* **2020**, *56*, 1126–1135. [CrossRef]
51. Ezema, I.C.; Aigbodion, V.S.; Okonkwo, E.G.; Obayi, C.S. Fatigue properties of value-added composite from Al-Si-Mg/palm kernel shell ash nanoparticles. *Int. J. Adv. Manuf. Technol.* **2020**, *107*, 3247–3257. [CrossRef]
52. Si, Y.; Di, W.; Liu, M.; Zhao, Y. Effects of pouring temperature and electromagnetic stirring on semi-solid microstructure of hypoeutectic Mg2Si/Al composite. *IOP Conf. Ser. Earth Environ. Sci.* **2021**, *692*, 32120. [CrossRef]
53. Zhang, Z.; Ge, B.; Xie, W.; Wei, Z.; Yang, W.; Li, Y.; Shi, Z. Effect of Si alloying content on the microstructure and thermophysical properties of SiC honeycomb/Al–Mg–Si composites prepared by spontaneous infiltration. *Ceram. Int.* **2020**, *46*, 10934–10941. [CrossRef]
54. Pan, J.; Liu, X.; He, G.; Ge, B.; Le, P.; Li, J.; Zhou, Z. Dry sliding tribological properties of A356-SiC aluminum matrix composites prepared by vacuum stir casting. *Ind. Lubr. Tribol.* **2021**, *73*, 685–691. [CrossRef]

55. Han, X.; Yang, L.; Zhao, N.; He, C. Copper-Coated Graphene Nanoplatelets-Reinforced Al–Si Alloy Matrix Composites Fabricated by Stir Casting Method. *Acta Metall. Sin. (Engl. Lett.)* **2021**, *34*, 111–124. [CrossRef]
56. Goudar, D.M.; Patil, I.S.; Magalad, V.T.; Rao, S.S.; Herbert, M.A. A comparative study of tensile properties of eutectic Al-Si/ZrO_2 composites fabricated by spray forming and stir casting methods. *Adv. Mater. Process. Technol.* **2022**, *8*, 2684–2698. [CrossRef]
57. Ramadoss, N.; Pazhanivel, K.; Anbuchezhiyan, G. Synthesis of B4C and BN reinforced Al7075 hybrid composites using stir casting method. *J. Mater. Res. Technol.* **2020**, *9*, 6297–6304. [CrossRef]
58. Tharanikumar, L.; Mohan, B.; Anbuchezhiyan, G. Enhancing the microstructure and mechanical properties of Si_3N_4–BN strengthened Al–Zn–Mg alloy hybrid nano composites using vacuum assisted stir casting method. *J. Mater. Res. Technol.* **2022**, *20*, 3646–3655. [CrossRef]
59. Pan, H.; He, Y.; Zhang, X. Interactions between Dislocations and Boundaries during Deformation. *Materials* **2021**, *14*, 1012. [CrossRef]
60. Yang, Z.; Fan, J.; Liu, Y.; Nie, J.; Yang, Z.; Kang, Y. Effect of the Particle Size and Matrix Strength on Strengthening and Damage Process of the Particle Reinforced Metal Matrix Composites. *Materials* **2021**, *14*, 675. [CrossRef]
61. Garg, P.; Jamwal, A.; Kumar, D.; Sadasivuni, K.K.; Hussain, C.M.; Gupta, P. Advance research progresses in aluminium matrix composites: Manufacturing & applications. *J. Mater. Res. Technol.* **2019**, *8*, 4924–4939. [CrossRef]
62. Farkash, A.; Mittelman, B.; Hayun, S.; Priel, E. Aluminum Matrix Composites with Weak Particle Matrix Interfaces: Effective Elastic Properties Investigated Using Micromechanical Modeling. *Materials* **2021**, *14*, 6083. [CrossRef] [PubMed]
63. Naik, S.N.; Walley, S.M. The Hall–Petch and inverse Hall–Petch relations and the hardness of nanocrystalline metals. *J. Mater. Sci.* **2020**, *55*, 2661–2681. [CrossRef]
64. Fu, B.; Pei, C.; Pan, H.; Guo, Y.; Fu, L.; Shan, A. Hall-Petch relationship of interstitial-free steel with a wide grain size range processed by asymmetric rolling and subsequent annealing. *Mater. Res. Express* **2020**, *7*, 116516. [CrossRef]
65. Fu, W.; Ma, J.; Liao, Z.; Xiong, H.; Fu, Y.; Wang, B. New Numerical Method Based on Linear Damage Evolution Law for Predicting Mechanical Properties of TiB(2)/6061Al. *Materials* **2023**, *16*, 4786. [CrossRef] [PubMed]
66. Sun, Y.; Zhao, Y.; Wu, J.; Kai, X.; Zhang, Z.; Fang, Z.; Xia, C. Effects of particulate agglomerated degree on deformation behaviors and mechanical properties of in-situ ZrB2 nanoparticles reinforced AA6016 matrix composites by finite element modelling. *Mater. Res. Express* **2020**, *7*, 36507. [CrossRef]
67. Bhowmik, A.; Dey, D.; Biswas, A. Microstructure, mechanical and wear Behaviour of AL7075/SIC Aluminium matrix composite fabricated by stir casting. *Indian J. Eng. Mater. Sci.* **2021**, *28*, 46–54. [CrossRef]
68. Gunawan; Arifin, A.; Irsyadi, Y.; Munandar, B.A. Effects of SiC particulate-reinforced on the fluidity and mechanical properties of Aluminium Matrix Composite through stir casting route. *J. Phys. Conf. Ser.* **2019**, *1198*, 32013. [CrossRef]
69. Aghajani, S.; Pouyafar, V.; Meshkabadi, R.; Volinsky, A.A.; Bolouri, A. Mechanical characterization of high volume fraction Al7075-Al2O3 composite fabricated by semisolid powder processing. *Int. J. Adv. Manuf. Technol.* **2023**, *125*, 2569–2580. [CrossRef]
70. Kermode, J.R.; Ben-Bashat, L.; Atrash, F.; Cilliers, J.J.; Sherman, D.; De Vita, A. Macroscopic scattering of cracks initiated at single impurity atoms. *Nat. Commun.* **2013**, *4*, 2441. [CrossRef]
71. Bellairu, P.K.; Bhat, S.; Gijo, E.V.; Poornesh, M. Multi-Response Modelling and Optimization of Agave Cantala Natural Fiber and Multi-wall Carbon Nano Tube Reinforced Polymer Nanocomposite: Application of Mixture Design. *Fibers Polym.* **2022**, *23*, 1089–1099. [CrossRef]

Disclaimer/Publisher's Note: The statements, opinions and data contained in all publications are solely those of the individual author(s) and contributor(s) and not of MDPI and/or the editor(s). MDPI and/or the editor(s) disclaim responsibility for any injury to people or property resulting from any ideas, methods, instructions or products referred to in the content.